frontiers | Frontiers in Materials

TYPE Original Research
PUBLISHED 23 December 2022
DOI 10.3389/fmats.2022.1089695

OPEN ACCESS

EDITED BY
Hongwei Tian,
Jilin University, China

REVIEWED BY
Jingxiang Zhao,
Harbin Normal University, China
Xiaoming Zhang,
Chinese Academy of Sciences, China

*CORRESPONDENCE
Zhe Zhang,
zhangzhe@bupt.edu.cn

†These authors have contributed equally to this work and share first authorship

SPECIALTY SECTION
This article was submitted to Energy Materials, a section of the journal Frontiers in Materials

RECEIVED 04 November 2022
ACCEPTED 09 December 2022
PUBLISHED 23 December 2022

CITATION
Yang J, Zhang Z, Sun S and Wang C (2022), Mo modified Co_3O_4 nanosheets array by a rapid quenching strategy for efficient oxygen evolution electrocatalysis. *Front. Mater.* 9:1089695. doi: 10.3389/fmats.2022.1089695

Mo modified Co_3O_4 nanosheets array by a rapid quenching strategy for efficient oxygen evolution electrocatalysis

Jiangping Yang[1†], Zhe Zhang[1†*], Siyuan Sun[2] and Cheng Wang[1]

[1]State Key Laboratory of Information Photonics and Optical Communications, School of Science, Beijing University of Posts and Telecommunications, Beijing, China, [2]Chinese Academy of Engineering Innovation Strategy, Beijing, China

The development of transition metal oxides (TMOs) as electrocatalysts for oxygen evolution reaction (OER) has the potential to surpass the performance of noble-metal-based catalysts. In this work, a quenching rapidly strategy was used to synthesize Mo-modified Co_3O_4 nanosheet arrays as advanced catalysts. The resulting Mo-Co_3O_4 electrodes showed superior activity and reaction kinetics, with an overpotential of only 341 mV to drive a current density of 100 mA cm^{-2} and a Tafel slope of 69.0 mV dec^{-1}. This improved performance is thought to be due to the formation of high-valence Co sites, which creates a synergistic effect. The ability to regulate the synthesis without causing obvious agglomeration and nucleation growth during annealing makes this method a promising approach for the design of other advanced functional materials.

KEYWORDS

transition metal oxides, nanosheets array, surface modification, quenching strategy, oxygen evolution reaction

1 Introduction

As more and more new energy productions come into play now, most people see the use of traditional energy as damaging to the environment (Jeffrey, et al., 2003; Zhang, 2017; Zhi, et al., 2017; Hu, et al., 2021). From the perspective of new energy acquisition, it is a great selection to use the electrochemical method to realize energy conversion technology with high efficiency and stability (Wang et al., 2015). Hydrogen production from the electrolysis of water, for example, consists of two half-cell reactions, the hydrogen evolution reaction (HER) at the cathode and the oxygen precipitation reaction (OER) at the anode, where the OER plays a crucial role (Sayed, 2018; Wu, 2018; He, 2019). The development of high activity/high stability/low-cost OER catalysts for large-scale production is an important issue for academia and the industry today (Suen 2017). Although RuO_2 and IrO_2 noble metal oxides are considered the most efficient OER electrocatalysts, their high costs, apparent scarcity, and low stability have greatly impeded their large-scale application as OER electrocatalysts (Tang et al., 2014; Mao et al., 2015; Yu, 2015; Zhao, 2017; Fang, 2018; Zang et al., 2018; Zhang, 2018; Liu Z. et al, 2019). Owing

to the scarcity and high costs of these noble metals, there has been an increasingly growing interest among researchers regarding the use of Earth-abundant elements for the development of efficient electrocatalysts for OER (Liu et al., 2020; Wang L. et al, 2018; Wang B. et al, 2018; Gong et al., 2018; Xu et al., 2018; Yu et al., 2019; Liu G. et al, 2019; Cai et al., 2019; Laguna-Bercero et al., 2019). Transition metal oxides, which contain variable valence metal oxidized redox couples, have recently been considered one promising alternative to noble-metal-based catalysts for efficient OER in alkaline media (Nai et al., 2017; Zheng et al., 2018; Li et al, 2018a; Li et al., 2018b). Numerous studies have confirmed that transition metals and their compounds can be used for electrocatalytic processes through phase transitions, defect generation and migration, and electronic valence changes (Xu H. et al, 2020; Bai et al., 2022). In electrocatalytic processes, transition metal catalysts have the advantage of quickly creating and stabilizing the active center, which can be helpful to reduce the overall energy consumption in the electrocatalytic process and improve the overall reaction stability (Xu Q. et al, 2020).

Nevertheless, the OER electrocatalytic behavior is greatly restricted by intrinsic activity and adsorption ability for active *O and *OOH species (Tan et al., 2019; Chen et al., 2020; Wang Z. et al, 2022). Experiments and theoretical calculations have revealed that adjusting the energy band structure and exposing novel active sites can be applied to regulate the adsorption ability for promoting electrocatalytic performance (Shen et al., 2022; Wang et al., 2019). Thereby, various strategies such as forming composites, doping, interface engineering, *etc.* are developed to improve these shortcomings (Lei et al., 2014; Wang Z. et al, 2018; Lu et al., 2019). Among these, surface modification can effectively improve the intrinsic activity of the active site by rapidly reconstructing low-potential barrier surfaces (Bai et al., 2022). In some cases, just a slight ions modification of an electrode results in a synergistic catalytic effect enhancing the rate of OER by orders of magnitude (Sadiek et al., 2012), which can introduce oxygen vacancies and mesoporous structures to adjust energy band structure and enhance the charge transfer capacity of the catalyst (Yang et al., 2021; Zhang et al., 2021).

To accomplish modification for improving electrocatalytic performance, some feasible methods were raised such as solvothermal, precipitation, molten salt, and magnetron sputtering (Zhu et al., 2019; Xu H. et al, 2020; Zhang et al., 2020; Fan et al., 2022), which either lead to inevitable agglomeration and nucleation growth or cost too much for mass production (Yang et al., 2021). It is pivotal to develop a succinct and low-cost strategy to maintain the uniformity of microstructure. Herein, we used a one-step quenching strategy that can precisely tailor the surface chemistry by rapid cooling to modify Mo cations on the cobalt oxide self-supporting electrodes (Ye et al., 2021; Liu et al., 2022). The Co_3O_4 modified by Mo cations (Mo-Co_3O_4) has no nucleation growth and remains highly uniform. Moreover, the Mo- Co_3O_4 electrode shows the best OER stability and catalytic activity among all samples, with a low over-potential of 341 mV to reach the current density of 100 mA cm^{-2} and a small Tafel slope of 69.0 mV dec^{-1}. It is believed that this process is suitable for industrial mass production with minimal pollution.

2 Experimental section

2.1 Materials

Cobalt nitrate hexahydrate ($Co(NO_3)_2{\cdot}6H_2O$, Sigma-Aldrich), Sodium nitrate ($NaNO_3$, Sigma-Aldrich), Molybdenum acetylacetonate ($[CH_3COCH = C(O-)CH_3]_2MoO_2$, Macklin), Sodium molybdate (Na_2MoO_4, Macklin), Sodium tungstate (Na_2WO_4, Macklin), Ammonium metavanadate (NH_4VO_3, Macklin), ethanol (C_2H_6O, Aladdin), deionized water and an ultrathin carbon film on holey carbon (400 mesh, Cu, Ted Pella Inc.) were used as received without any further purification.

2.2 Materials synthesis

2.2.1 $Co(OH)_2$ precursors synthesis

$Co(OH)_2$ precursors were obtained by loading Co onto the substrate using electrodeposition: the 1*2 cm^2 nickel foam substrate was all immersed in an electrolyte consisting of 0.1 M cobalt nitrate and 0.01 M sodium nitrate, which was electrostatically anodized at 2 mA cm^{-2} to achieve 1,200 s of cobalt hydroxide deposition on the nickel foam substrate evenly.

2.2.2 Molybdenum cation modification

The $Co(OH)_2$ loaded on nickel foam (10 mm*20 mm*1.1 mm) was taken directly into a muffle furnace (stable at 250°C) and held for 5 min to obtain Co_3O_4. Next, the high-temperature Co_3O_4 was rapidly placed in a molybdenum solution (Molybdenum cation) of acetylacetonate at a concentration of 0.2 mg ml^{-1} at low temperatures (−40°C, −20°C, 0°C, and 20°C). Then, we kept it in a molybdenum solution of acetylacetonate under low temperatures for 10 min to obtain molybdenum-modified Co_3O_4 (Mo-Co_3O_4) by quenching. Finally, we used deionized water and ethanolic to rinse all samples and then dried them at room temperature.

2.3 Characterization

An X-ray diffractometer (XRD, D/max 2500 V) was used to investigate the crystal structure of the samples. We used a scanning electron microscope (SEM, Zeiss Ultra Plus), and transmission electron microscopy (TEM, JEM-2100F, Japan) to analyze the microstructure of samples. The distribution of elements in Mo-Co_3O_4 was obtained by the energy dispersive spectrometer (EDS). X-ray photoelectron spectroscopy (XPS, Escalab 250 Xi) was used to study the surface chemistry of these samples.

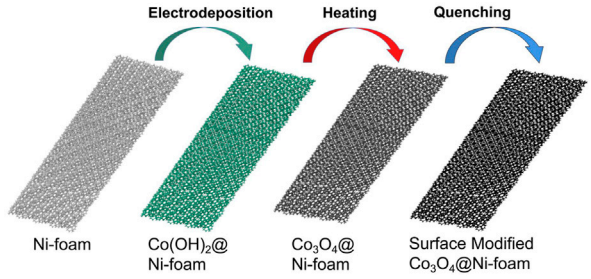

FIGURE 1
Schematic illustration of the preparation process of samples.

2.4 Electrochemical measurements

All electro-catalytic tests were conducted in a conventional three-electrode electrochemical system containing 1 M KOH solution electrolyte at room temperature, using an Autolab PGSTAT-204 potentiostat equipped with the Nova 2.13 software. The counter electrode and reference electrodes are graphite rod and Hg/HgO (filling with 1M KOH) respectively. The potential of the Hg/HgO reference electrode was regularly calibrated in potassium hydroxide solution before the experiments. All potentials applied herein were calibrated to the RHE using the following equation: $E_{RHE} = E_{Hg/HgO}+0.098 + 0.059 \times pH$. The loading of the commercial catalyst IrO_2 is 48 μg cm^{-2}. Before LSV measurements, the catalyst had been activated with the scan rate of 50 mV s^{-1} for at least 50 cycles until stable cyclic voltammetry (CV) curves were obtained in the test range while Tafel slopes were derived from the LSV curves. Stability evaluation was performed by its chronoamperometric response, which was implemented at a current density of about 50 mA cm^{-2}. The accelerated durability test (ADT) was carried out at the voltage range of 1.10–1.60 V (vs. RHE) for 5,000 cyclic voltammetry cycles with a scan rate of 100 mV s^{-1}. Nyquist plots were obtained from EIS measurements at 1.6 V (vs. RHE) in N2-saturated electrolytes. Chrono analysis (CA) test was further carried out at a constant voltage of 1.5 V vs. RHE in 1 M N_2-saturated KOH for 24h.

3 Results and discussion

3.1 Material structure

The preparation flow of the synthetic Mo ion-modified cobalt hydroxide electrode is shown in Figure 1. The growth of cobalt hydroxide nanoarrays on a nickel foam substrate skeleton is first completed at the anode by conventional electrodeposition. The $Co(OH)_2$ loaded on nickel foam was taken directly into a muffle furnace to obtain Co_3O_4. Next, the high-temperature Co_3O_4 was rapidly placed in a molybdenum solution (Molybdenum cation) of acetylacetonate at low temperatures. Then, we kept it in the molybdenum solution of acetylacetonate under low temperatures to obtain molybdenum-modified Co_3O_4 (Mo-Co_3O_4) by quenching. For comparison, we also involved anions containing high-valence metals modification by just changing the quenching precursor solution corresponding to Tungsten or Vanadium cation of acetylacetonate and sodium molybdate solution. And we labeled the corresponding samples modified by different ions as W-Co_3O_4, V-Co_3O_4, and A-Mo-Co_3O_4.

Two main factors affect the quenching strategy: heating temperature and cooling temperature. Scanning electron microscopy (SEM) was used to further observe the surface morphology of the electrode material. A series of experimental investigations about heating temperature has been done (Supplementary Figure S1), which shows that 250°C heating maintains the original spatial structure of the catalyst stably and regularly. We designed a series of cooling temperature gradients to investigate the effects of low temperatures, therefore. Under 250°C heating temperature, the nanosheets of the sample microstructure grow into disorder and the uniformity of the array decreases (Figure 2) slightly as the temperature of the precursor solution increases. When the precursor solution temperature is at room temperature (−20°C) conditions, the microscopic structure of the material appears significantly irregular. Besides, the EDS elemental mapping pictures (Supplementary Figure S2) of Mo-Co_3O_4 confirm that Co, Mo, and O elements are uniformly distributed throughout the nanosheets.

High-angle annular dark field (HAADF) and TEM images (Figures 3A,B) show the micro-morphology of Mo-Co_3O_4 (heated at 250°C, cooled at −40°C). Clear lattice fringes with interplanar spacings of 0.147 nm and 0.245 nm are observed from high-resolution TEM (HR-TEM) images (Figure 3C), respectively. Besides, the selected area electron diffraction (SAED) pattern shows marked diffraction rings corresponding to (220), (311), and (400) planes of the Co_3O_4 phase (Figure 3D). The result confirms that the Mo-Co_3O_4 still well maintains the Co_3O_4 structure, and such microstructure possesses nanoscale grains with a high density of grain boundaries, which could contribute to many active sites for catalytic reactions (Yu et al., 2015). The crystalline phase of the sample (Mo-Co_3O_4) is characterized by X-ray powder diffraction (XRD) to monitor the possible structure and morphology changes induced by ions modification (Figure 4A). To eliminate the strong background of Ni foam substrate, we further amplify the XRD pattern as shown in Figure 4B, which shows the XRD diffraction peaks of samples all can be well indexed to pure Co_3O_4 (JCPDS card No. 43–1,003). There are no additional peaks ascribed to molybdenum phases or compounds after modification, suggesting this method did not convert the structure of the Co_3O_4.

X-ray photoelectron spectroscopy (XPS) further examines the surface chemical composition of samples. Four typical peaks corresponding to the binding energies of Mo 3 days, O 1 s, Co 2p, and Ni 2p can be observed in Figure 4C. Regarding the Co 2p

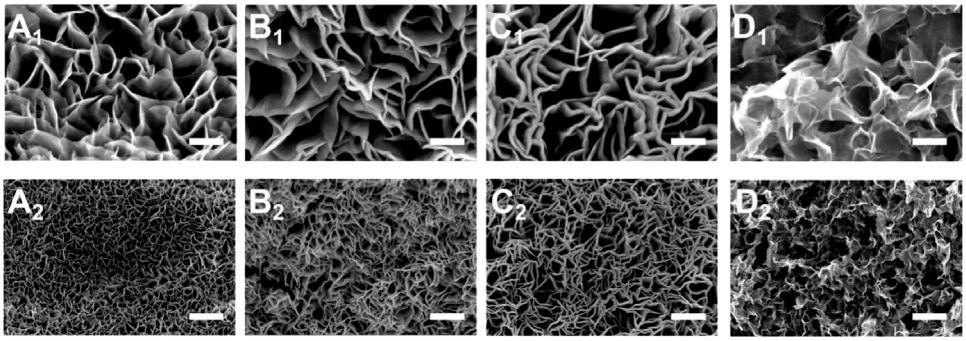

FIGURE 2
SEM images of Mo-Co_3O_4 for different cooling temperatures in the quenching strategy (scale bar: 1: 100 nm; 2: 1 μm; **(A)** 40°C; **(B)** 20°C; **(C)** 0°C; **(D)** 20°C).

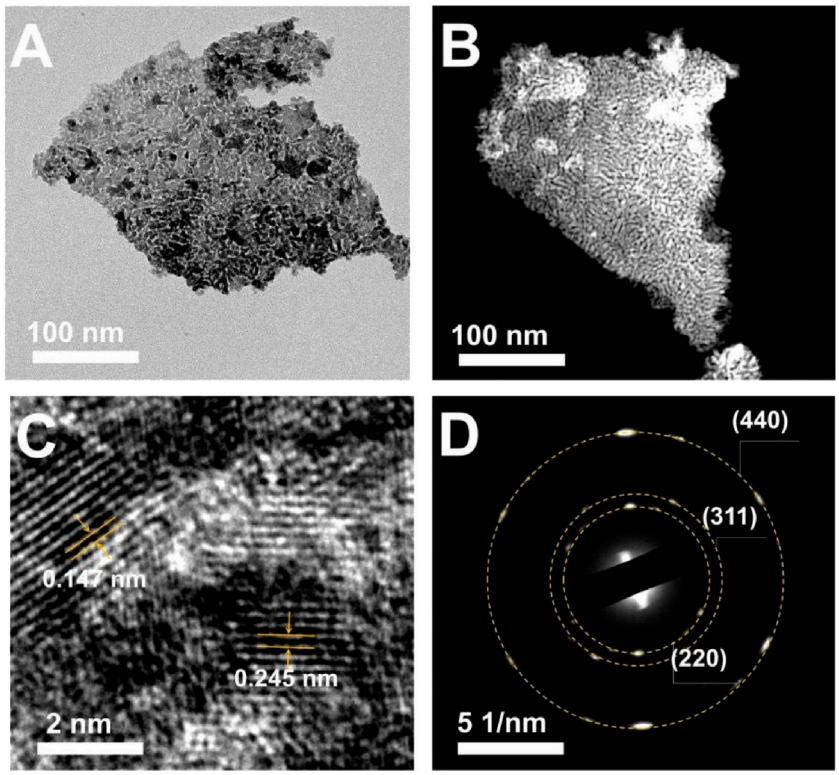

FIGURE 3
(A) TEM and **(B)** SEM images of Mo-Co_3O_4 (heated at 250°C, cooled at −40°C). **(C)** HRTEM and **(D)** the corresponding Fourier transform (FFT) patterns of Mo-Co_3O_4 (heated at 250°C, quenched at −40°C).

region in samples, the existence of two fitting peaks belongs to Co 2p3/2 and Co 2p1/2 (Figure 4D) with binding energies at 781.5 and 797.4 eV (Huang et al., 2020). It is noteworthy that the binding energy of Co species increased after Mo modification. And the induced high valence Co is deemed to increase intrinsic activity (Guan et al., 2018; Kou et al., 2020). As shown in Figure 4E, the XPS spectrum of O 1s can be deconvoluted into three pairs of 529.8, 531.3, and 533.3 eV, which can be attributed to the lattice oxygen (O1), coordinative oxygen vacancy or hydroxyl group (O2) and adsorbed H_2O (O3), respectively (Gao et al., 2019; Bao et al., 2015; Zhuang et al., 2017). For Mo-Co_3O_4, the O2's relative enhancement suggested Mo cation surface modification will

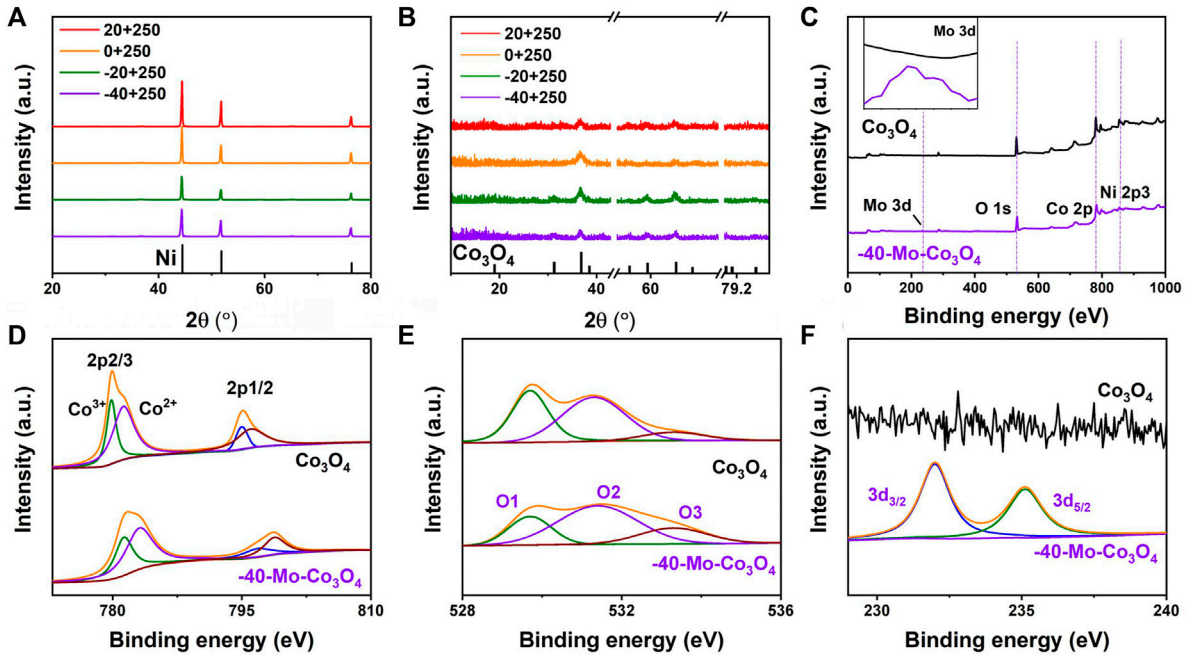

FIGURE 4
(A,B) XRD patterns of Mo-Co_3O_4 at different cooling temperatures (heated at 250°C), **(C)** XPS spectra of survey for Co_3O_4 and Mo-Co_3O_4 (heated at 250°C, quenched at -40°C), XPS spectra of **(D)** Co 2p, **(E)** O 1s, and **(F)** Mo 3 days for Mo-Co_3O_4 (heated at 250°C, quenched at −40°C).

produce a large concentration of oxygen vacancies and boost the adsorption/desorption of the OH group (Yang et al., 2017; Ran et al., 2020). This would be beneficial to regulating the ΔG of OH* adsorption/desorption, thus accelerating the kinetic process and finally enhancing the OER activity (Greeley et al., 2006). For Mo 3 days spectrum (Figure 4F), the Mo 3 days peaks of Mo-Co_3O_4 correspond to Mo 3d3/2 (232.3 eV) and Mo 3d5/2 (235.2 eV), demonstrating that Mo was successfully adsorbed into nanosheets. Compared with the binding energies of the Mo precursor (Supplementary Figure S3), the binding energy of Mo species decreased after modification (Wang T. et al, 2022), confirming the electron interaction between Co and Mo species.

3.2 Electrorheological property

The polarization curves after iR-compensation were obtained by linear sweep voltammetry (LSV) at a scan rate of 5 mV s^{-1} for all samples. The modifying reaction temperature plays an important role in the OER activity of the catalyst. Taking Mo-Co_3O_4 as an example, we first confirmed that the sample obtained at a heating temperature of 250°C had the best electrochemical performance (Supplementary Figure S4). Under the fixed healing temperature of 250°C, as the temperature of the precursor solution increases (−40°C, −20°C, 0°C, 20°C), the samples reach the current density of 100 mA cm^{-2} at overpotentials of 341, 356, 373, and 390 mV. In addition, the Tafel slopes of the corresponding electrodes were 69.0 mV dec^{-1}, 91.1 mV dec^{-1}, 114.6 mV dec^{-1}, 146.2 mV dec^{-1} (Figure 5B), indicating that Mo-Co_3O_4 quenched at -40°C had better electro-catalytic property and OER-kinetics than other as-synthesized materials catalysts. To further explore the role of molybdenum ions in different valence states, our design uses sodium molybdate solution as a precursor to synthesize. As shown in Figures 5D,E, under the same modifying condition (heated under 250°C and quenched under −40°C), Mo-Co_3O_4 exhibited a remarkably electro-catalytic property, which is better than Co_3O_4 modified by molybdenum acid ions (named A-Mo-Co_3O_4) and bare Co_3O_4 sample. Besides, the Mo-Co_3O_4 electrode (heated under 250°C, quenched under −40°C) exhibits the smallest semicircle associated with charge transfer resistance, which indicates optimal electrochemical kinetics (Figures 3C,F, Supplementary Figure S5 and Supplementary Table S1). The electrochemical double layer capacitance (C_{dl}) is to evaluate the electrochemically active surface areas (ECSA) by measuring the cyclic voltammetry curve of the samples prepared in the range at different scan rates (10, 20, 30, 40, 50 mV s^{-1}). The corresponding CV curves are shown in Supplementary Figure S9, meanwhile, the calculation of C_{dl} (Supplementary Figures S7, S8) shows the Mo-Co_3O_4 (heated under 250°C, quenched under −40°C) sample reaches the largest value of 44.85 mF cm^{-2}. The ECSA calculated from C_{dl}-EIS follows a similar trend as the OER catalytic activity, and Mo-Co_3O_4 (heated under 250°C, quenched under −40°C) owns the largest ECSA value, which means the Mo-Co_3O_4 (heated under 250°C, quenched under −40°C) sample can expose the most active sites to the

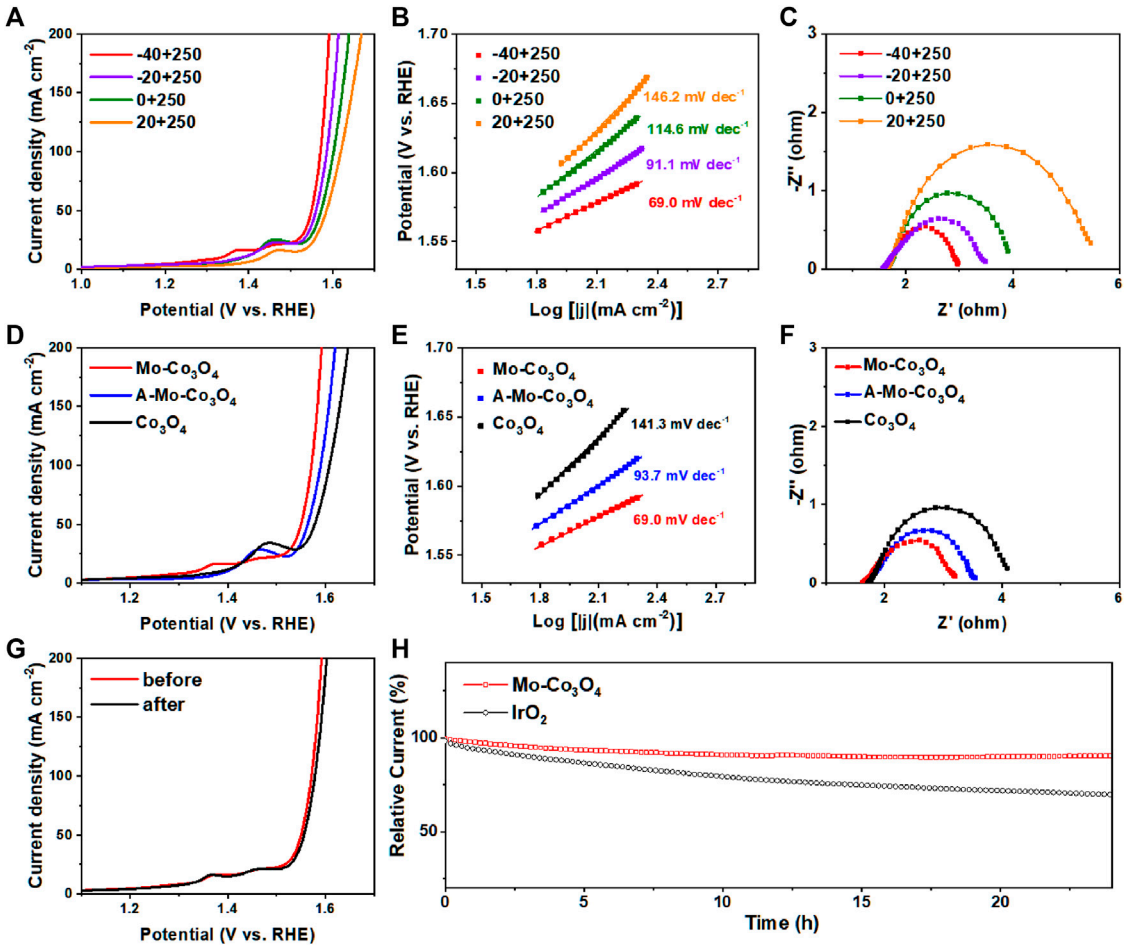

FIGURE 5
(A) LSV curves, **(B)** Tafel plots and **(C)** Nyquist plots obtained from EIS measurements at 1.6 V (vs. RHE) of Mo-Co_3O_4 electrodes with different cooling temperatures (−40°C, -20°C, 0°C and 20°C), all were heated under 250°C. **(D)** LSV curves, **(E)** Tafel plots and **(F)** Nyquist plots were obtained from EIS measurements at 1.6 V (vs. RHE) of Mo-Co_3O_4 electrodes with different annealing temperatures (Mo-Co_3O_4, A-Mo-Co_3O_4 and Co_3O_4 heat treatment only). **(G)** Stability tests by ADT method for Mo-Co_3O_4 (heated under 250°C and quenched under -40°C), where polarization curves are recorded before and after 5000 CV cycles. **(H)** Chronoamperometry curves of Mo-Co_3O_4 (heated under 250°C and quenched under −40°C) and commercial IrO_2.

electrolyte during OER among all samples. Furthermore, we tested the modification function of different high valence metal ions (modified through different quenching precursor solutions we called Mo-Co_3O_4, W-Co_3O_4, V-Co_3O_4, A-Mo-Co_3O_4, and commercial IrO_2) as a contrast (Supplementary Figures S6, S10), and Co_3O_4 catalyst modified by Mo cation had a better performance. Mo-Co_3O_4 (heated under 250°C, quenched under −40°C) has competitive advantages in catalytic activity and Tafel kinetics over related literature (Supplementary Table S2).

The improvement observed in the OER electrocatalytic properties of the Mo-Co_3O_4 electrode is attributed to the synergistic effects of the binary metal ions, including Co and Mo (Yang et al., 2018b; Yang L. J. et al, 2018; Bezerra et al., 2020; Guirguis et al., 2020), which acted as active sites. Furthermore, the metal/ions−support interactions (geometric effects, charge transfer) and the interaction between the different oxides resulted in better OER catalysis (Gerber et al., 2019; Bezerra et al., 2020) for the Mo-Co_3O_4 catalyst. It is worth noting that the microstructure of the sample after modification (heated under 250°C and quenched under −40°C) does not appear to noticeable change, which provides stable reaction space and thus provides excellent stability. Figure 5G shows the stability of the electrode investigated by the ADT test, with negligible degradation after 5000 CV cycles. The OER activity of the sample decreased by less than 5% after 24 h of the constant current test (Figure 5H). Obtained under suitable reaction temperatures, the Mo-Co_3O_4 catalysts have a more uniform and regular microstructure which leads to better stability.

4 Conclusion

In the present work, we promoted Co_3O_4 by a surface modification to obtain a cheap and industrially productive electrode for OER. On the one hand, the incorporation of high valence Mo cations brought a synergistic effect with Co and modified electron interaction. On the other hand, the quenching method sustained surface microstructure without heating agglomeration and nucleation growth, which is also advantageous to electrochemical properties. The best sample was obtained at a heating temperature of 250°C and a cooling temperature of −40°C with Mo cation modified, compared to samples modified in other synthetic temperature conditions. Our self-supported Mo-Co_3O_4 electrode avoids the use of expensive polymer binders to fix active material to the substrate. This work provides a valuable strategy to modify the electronic structure and OER catalytic performance of TMO, which obtains better OER activation (Wang et al., 2019; Li et al., 2018b; Yang J. et al., 2018; Zheng et al., 2018; Yu et al., 2019; Liu et al., 2020; Fan et al., 2022).

Data availability statement

The original contributions presented in the study are included in the article/Supplementary Material, further inquiries can be directed to the corresponding author.

Author contributions

JY: Data curation, investigation, and writing-original draft; ZZ: Data curation, investigation, methodology, and writing—original draft, review and editing; SS: validation, and conceptualization; CW: validation, and conceptualization.

Acknowledgments

We acknowledge the financial support from the Fund of National Natural Science Foundation of China (Grant No. U2241243), State Key Laboratory of Information Photonics and Optical Communications (Beijing University of Posts and Telecommunications, P.R. China), Guangdong Hydrogen Energy Institute of WHUT under Guangdong Key Areas Research and Development Program (2019B090909003), Foshan Xianhu Laboratory of the Advanced Energy Science and Technology Guangdong Laboratory under Open-end Funds (XHD2020-004).

Conflict of interest

The authors declare that the research was conducted in the absence of any commercial or financial relationships that could be construed as a potential conflict of interest.

Publisher's note

All claims expressed in this article are solely those of the authors and do not necessarily represent those of their affiliated organizations, or those of the publisher, the editors and the reviewers. Any product that may be evaluated in this article, or claim that may be made by its manufacturer, is not guaranteed or endorsed by the publisher.

Supplementary material

The Supplementary Material for this article can be found online at: https://www.frontiersin.org/articles/10.3389/fmats.2022.1089695/full#supplementary-material

References

Bai, J., Mei, J., Liao, T., Sun, Q., Chen, Z. G., and Sun, Z. (2022). Molybdenum-promoted surface reconstruction in polymorphic cobalt for initiating rapid oxygen evolution. *Adv. Energy Mat.* 12 (5), 2103247. doi:10.1002/aenm.202103247

Bao, J., Zhang, X., Fan, B., Zhang, J., Zhou, M., Yang, W., et al. (2015). Ultrathin spinel-structured nanosheets rich in oxygen deficiencies for enhanced electrocatalytic water oxidation. *Angew. Chem.* 127 (25), 7507–7512. doi:10.1002/ange.201502226

Bezerra, L. S., and Maia, G. (2020). Developing efficient catalysts for the OER and ORR using a combination of Co, Ni, and Pt oxides along with graphene nanoribbons and $NiCo_2O_4$. *J. Mat. Chem. A* 8 (34), 17691–17705. doi:10.1039/D0TA05908K

Cai, M., Lu, X., Zou, Z., Guo, K., Xi, P., and Xu, C. (2019). The energy level regulation of CoMo carbonate hydroxide for the enhanced oxygen evolution reaction activity. *ACS Sustain. Chem. Eng.* 7 (6), 6161–6169. doi:10.1021/acssuschemeng.8b06360

Chen, X., Chen, Y., Luo, X., Guo, H., Wang, N., Su, D., et al. (2020). Polyaniline engineering defect-induced nitrogen doped carbon-supported Co3O4 hybrid composite as a high-efficiency electrocatalyst for oxygen evolution reaction. *Appl. Surf. Sci.* 526, 146626. doi:10.1016/j.apsusc.2020.146626

Fan, M., Cui, L., He, X., and Zou, X. (2022). Emerging heterogeneous supports for efficient electrocatalysis. *Small Methods* 6, 2200855. doi:10.1002/smtd.202200855

Fang, L., Wang, F., Zhai, T., Qiu, Y., Lan, M., Huang, K., et al. (2018). Hierarchical CoMoO4 nanoneedle electrodes for advanced supercapacitors and electrocatalytic oxygen evolution. *Electrochim. Acta* 259, 552–558. doi:10.1016/j.electacta.2017.11.012

Gao, J., Xu, C. Q., Hung, S. F., Liu, W., Cai, W., Zeng, Z., et al. (2019). Breaking long-range order in iridium oxide by alkali ion for efficient water oxidation. *J. Am. Chem. Soc.* 141 (7), 3014–3023. doi:10.1021/jacs.8b11456

Gerber, I. C., and Serp, P. (2019). A theory/experience description of support effects in carbon-supported catalysts. *Chem. Rev.* 120 (2), 1250–1349. doi:10.1021/acs.chemrev.9b00209

Gong, Y., Yang, Z., Lin, Y., Wang, J., Pan, H., and Xu, Z. (2018). Hierarchical heterostructure $NiCo_2O_4$@ $CoMoO_4$/NF as an efficient bifunctional electrocatalyst for overall water splitting. *J. Mat. Chem. A* 6 (35), 16950–16958. doi:10.1039/C8TA04325F

Greeley, J., Jaramillo, T. F., Bonde, J., Chorkendorff, I. B., and Nørskov, J. K. (2006). Computational high-throughput screening of electrocatalytic materials for hydrogen evolution. *Nat. Mat.* 5 (11), 909–913. doi:10.1038/nmat1752

Guan, C., Xiao, W., Wu, H., Liu, X., Zang, W., Zhang, H., et al. (2018). Hollow Mo-doped CoP nanoarrays for efficient overall water splitting. *Nano Energy* 48, 73–80. doi:10.1016/j.nanoen.2018.03.034

Guirguis, A., Maina, J. W., Zhang, X., Henderson, L. C., Kong, L., Shon, H., et al. (2020). Applications of nano-porous graphene materials–critical review on performance and challenges. *Mat. Horiz.* 7 (5), 1218–1245. doi:10.1039/C9MH01570A

He, X., Luan, S. Z., Wang, L., Wang, R. Y., Du, P., Xu, Y. Y., et al. (2019). Facile loading mesoporous Co3O4 on nitrogen doped carbon matrix as an enhanced oxygen electrode catalyst. *Mat. Lett.* 244, 78–82. doi:10.1016/j.matlet.2019.01.144

Hu, N., Du, Jing., Ma, Yuan-Yuan., Cui, W. J., Yu, B. R., Han, Z. G., et al. (2021). Unravelling the role of polyoxovanadates in electrocatalytic water oxidation reaction: Active species or precursors. *Appl. Surf. Sci.* 540, 148306. doi:10.1016/j.apsusc.2020.148306

Huang, K., Guo, S., Wang, R., Lin, S., Hussain, N., Wei, H., and Wu, H. (2020). Two-dimensional MOF/MOF derivative arrays on nickel foam as efficient bifunctional coupled oxygen electrodes. *Chin. J. Catal.* 41 (11), 1754–1760. doi:10.1016/S1872-2067(20)63613-0

Jeffrey, C., Kopp, R. J., and Portney, P. R. (2003). Energy resources and global development. *Science* 302, 1528–1531. doi:10.1126/science.1091939

Kou, Z., Yu, Y., Liu, X., Gao, X., Zheng, L., Zou, H., et al. (2020). Potential-dependent phase transition and Mo-enriched surface reconstruction of γ-CoOOH in a heterostructured Co-Mo_2C precatalyst enable water oxidation. *ACS Catal.* 10 (7), 4411–4419. doi:10.1021/acscatal.0c00340

Laguna-Bercero, M. A., Orera, A., Morales-Zapata, M., and Larrea, A. (2019). Development of advanced nickelate-based oxygen electrodes for solid oxide cells. *ECS Trans.* 91 (1), 2409–2416. doi:10.1149/09101.2409ecst

Lei, F., Sun, Y., Liu, K., Gao, S., Liang, L., Pan, B., et al. (2014). Oxygen vacancies confined in ultrathin indium oxide porous sheets for promoted visible-light water splitting. *J. Am. Chem. Soc.* 136 (19), 6826–6829. doi:10.1021/ja501866r

Li, Y., Xu, H., Huang, H., Wang, C., Gao, L., and Ma, T. (2018a). One-dimensional MoO_2–$Co_2Mo_3O_8$@ C nanorods: A novel and highly efficient oxygen evolution reaction catalyst derived from metal–organic framework composites. *Chem. Commun.* 54 (22), 2739–2742. doi:10.1039/C8CC00025E

Li, Y. J., Cui, L., Da, P. F., Qiu, K. W., Qin, W. J., Hu, W. B., et al. (2018b). Multiscale structural engineering of Ni-doped CoO nanosheets for zinc–air batteries with high power density. *Adv. Mat.* 30 (46), 1804653. doi:10.1002/adma.201804653

Liu, G., Bai, H., Ji, Y., Wang, L., Wen, Y., Lin, H., et al. (2019b). A highly efficient alkaline HER Co–Mo bimetallic carbide catalyst with an optimized Mo d-orbital electronic state. *J. Mat. Chem. A* 7 (20), 12434–12439. doi:10.1039/C9TA02886B

Liu, R., Anjass, M., Greiner, S., Liu, S., Gao, D., Biskupek, J., et al. (2020). Bottom-up design of bimetallic cobalt–molybdenum carbides/oxides for overall water splitting. *Chem. Eur. J.* 26 (18), 4157–4164. doi:10.1002/chem.201905265

Liu, T., Yang, S., Guan, J., Niu, J., Zhang, Z., and Wang, F. (2022). Quenching as a route to defect-rich Ru-pyrochlore electrocatalysts toward the oxygen evolution reaction. *Small Methods* 6 (1), 2101156. doi:10.1002/smtd.202101156

Liu, Z., Zhan, C., Peng, L., Cao, Y., Chen, Y., Ding, S., et al. (2019a). A CoMoO 4–Co 2 Mo 3 O 8 heterostructure with valence-rich molybdenum for a high-performance hydrogen evolution reaction in alkaline solution. *J. Mat. Chem. A* 7 (28), 16761–16769. doi:10.1039/C9TA04180J

Lu, X. F., Chen, Y., Wang, S., Gao, S., and Lou, X. W. (2019). Interfacing manganese oxide and cobalt in porous graphitic carbon polyhedrons boosts oxygen electrocatalysis for Zn–air batteries. *Adv. Mat.* 31 (39), 1902339. doi:10.1002/adma.201902339

Mao, S., Wen, Z., Ci, S., Guo, X., Ostrikov, K., and Chen, J. (2015). Perpendicularly oriented MoSe2/graphene nanosheets as advanced electrocatalysts for hydrogen evolution. *Small* 11 (4), 414–419. doi:10.1002/smll.201401598

Nai, J., Lu, Y., Yu, L., Wang, X., and Lou, X. W. (2017). Formation of Ni–Fe mixed diselenide nanocages as a superior oxygen evolution electrocatalyst. *Adv. Mat.* 29 (41), 1703870. doi:10.1002/adma.201703870

Ran, J., Wang, T., Zhang, J., Liu, Y., Xu, C., Xi, S., et al. (2020). Modulation of electronics of oxide perovskites by sulfur doping for electrocatalysis in rechargeable Zn–air batteries. *Chem. Mat.* 32 (8), 3439–3446. doi:10.1021/acs.chemmater.9b05148

Sadiek, I. M., Mohammad, A. M., El-Shakre, M. E., and El-Deab, M. S. (2012). Electrocatalytic activity of nickel oxide nanoparticles-modified electrodes: Optimization of the loading level and operating pH towards the oxygen evolution reaction. *Int. J. Hydrog. Energy.* 37 (1), 68–77. doi:10.1016/j.ijhydene.2011.09.097

Sayed, D. M., El-Nagar, G. A., Sayed, S. Y., El-Anadouli, B. E., and El-Deab, M. S. (2018). Activation/deactivation behavior of nano-NiOx based anodes towards the OER: Influence of temperature. *Electrochimica Acta* 276, 176–183. doi:10.1016/j.electacta.2018.04.175

Shen, S., Hu, Z., Zhang, H., Song, K., Wang, Z., Lin, Z., et al. (2022). Highly active Si sites enabled by negative valent Ru for electrocatalytic hydrogen evolution in LaRuSi. *Angew. Chem. Int. Ed.* 134 (32), e202206460. doi:10.1002/anie.202206460

Suen, N. T., Hung, S. F., Quan, Q., Zhang, N., Xu, Y. J., and Chen, H. M. (2017). Electrocatalysis for the oxygen evolution reaction: Recent development and future perspectives. *Chem. Soc. Rev.* 46, 337–365. doi:10.1039/C6CS00328A

Tan, P., Chen, B., Xu, H., Cai, W., He, W., and Ni, M. (2019). *In-situ* growth of Co_3O_4 nanowire-assembled clusters on nickel foam for aqueous rechargeable Zn-Co3O4 and Zn-air batteries. *Appl. Catal. B Environ.* 241, 104–112. doi:10.1016/j.apcatb.2018.09.017

Tang, H., Dou, K., Kaun, C. C., Kuang, Q., and Yang, S. (2014). $MoSe_2$ nanosheets and their graphene hybrids: Synthesis, characterization and hydrogen evolution reaction studies. *J. Mat. Chem. A* 2 (2), 360–364. doi:10.1039/C3TA13584E

Wang, L., Zhou, Q., Pu, Z., Zhang, Q., Mu, X., Jing, H., et al. (2018a). Surface reconstruction engineering of cobalt phosphides by Ru inducement to form hollow Ru-RuPx-CoxP pre-electrocatalysts with accelerated oxygen evolution reaction. *Nano Energy* 53, 270–276. doi:10.1016/j.nanoen.2018.08.061

Wang, B., Wang, Z., Wang, X., Zheng, B., Zhang, W., and Chen, Y. (2018b). Scalable synthesis of porous hollow CoSe 2–Mose 2/carbon microspheres for highly efficient hydrogen evolution reaction in acidic and alkaline media. *J. Mat. Chem. A* 6 (26), 12701–12707. doi:10.1039/C8TA03523G

Wang, T., Chen, H. C., Yu, F., Zhao, X. S., and Wang, H. (2019). Boosting the cycling stability of transition metal compounds-based supercapacitors. *Energy Storage Mater.* 16, 545–573. doi:10.1016/j.ensm.2018.09.007

Wang, T., Wang, P., Zang, W., Li, X., Chen, D., Kou, Z., et al. (2022b). Nanoframes of Co_3O_4–Mo_2N heterointerfaces enable high-performance bifunctionality toward both electrocatalytic HER and OER. *Adv. Funct. Mat.* 32 (7), 2107382. doi:10.1002/adfm.202107382

Wang, Z., Liu, H., Ge, R., Ren, X., Ren, J., Yang, D., et al. (2018c). Phosphorus-doped Co_3O_4 nanowire array: A highly efficient bifunctional electrocatalyst for overall water splitting. *ACS Catal.* 8 (3), 2236–2241. doi:10.1021/acscatal.7b03594

Wang, Z., Shen, S., Lin, Z., Tao, W., Zhang, Q., Meng, F., et al. (2022a). Regulating the local spin state and band structure in Ni3S2 nanosheet for improved oxygen evolution activity. *Adv. Funct. Mat.* 32, 2112832. doi:10.1002/adfm.202112832

Wu, A., Xie, Y., Ma, H., Tian, C., Gu, Y., Yan, H., et al. (2018). Integrating the active OER and HER components as the heterostructures for the efficient overall water splitting. *Nano Energy* 44, 353–363. doi:10.1016/j.nanoen.2017.11.045

Xu, H., Fei, B., Cai, G., Ha, Y., Liu, J., Jia, H., et al. (2020a). Boronization-induced ultrathin 2D nanosheets with abundant crystalline–amorphous phase boundary supported on nickel foam toward efficient water splitting. *Adv. Energy Mat.* 10 (3), 1902714. doi:10.1002/aenm.201902714

Xu, Q., Jiang, H., Duan, X., Jiang, Z., Hu, Y., Boettcher, S. W., et al. (2020b). Fluorination-enabled reconstruction of NiFe electrocatalysts for efficient water oxidation. *Nano Lett.* 21 (1), 492–499. doi:10.1021/acs.nanolett.0c03950

Xu, Y., Xie, L., Li, D., Yang, R., Jiang, D., and Chen, M. (2018). Engineering Ni $(OH)_2$ nanosheet on $CoMoO_4$ nanoplate array as efficient electrocatalyst for oxygen evolution reaction. *ACS Sustain. Chem. Eng.* 6 (12), 16086–16095. doi:10.1021/acssuschemeng.8b02663

Yang, G., Zhu, B., Fu, Y., Zhao, J., Lin, Y., Gao, D., et al. (2021). High-valent Zirconium-doping modified Co_3O_4 weave-like nanoarray boosts oxygen evolution reaction. *J. Alloys Compd.* 886, 161172. doi:10.1016/j.jallcom.2021.161172

Yang, J., Yu, C., Hu, C., Wang, M., Li, S., Huang, H., et al. (2018b). Surface-confined fabrication of ultrathin nickel cobalt-layered double hydroxide nanosheets for high-performance supercapacitors. *Adv. Funct. Mat.* 28 (44), 1803272. doi:10.1002/adfm.201803272

Yang, L. J., Deng, Y. Q., Zhang, X. F., Liu, H., and Zhou, W. J. (2018a). $MoSe_2$ nanosheet/MoO_2 nanobelt/carbon nanotube membrane as flexible and multifunctional electrodes for full water splitting in acidic electrolyte. *Nanoscale* 10 (19), 9268–9275. doi:10.1039/C8NR01572D

Yang, Y., Zhang, K., Lin, H., Li, X., Chan, H. C., Yang, L., et al. (2017). MoS_2–Ni_3S_2 heteronanorods as efficient and stable bifunctional electrocatalysts for overall water splitting. *ACS Catal.* 7 (4), 2357–2366. doi:10.1021/acscatal.6b03192

Ye, C., Liu, J., Zhang, Q., Jin, X., Zhao, Y., Pan, Z., et al. (2021). Activating metal oxides nanocatalysts for electrocatalytic water oxidation by quenching-induced near-surface metal atom functionality. *J. Am. Chem. Soc.* 143 (35), 14169–14177. doi:10.1021/jacs.1c04737

Yu, M., Belthle, K. S., Tüysüz, C., and Tüysüz, H. (2019). Selective acid leaching: A simple way to engineer cobalt oxide nanostructures for the electrochemical oxygen evolution reaction. *J. Mat. Chem. A* 7 (40), 23130–23139. doi:10.1039/C9TA07835E

Yu, M. Q., Jiang, L. X., and Yang, H. G. (2015). Ultrathin nanosheets constructed CoMoO 4 porous flowers with high activity for electrocatalytic oxygen evolution. *Chem. Commun.* 51 (76), 14361–14364. doi:10.1039/C5CC05511C

Zang, M., Xu, N., Cao, G., Chen, Z., Cui, J., Gan, L., et al. (2018). Cobalt molybdenum oxide derived high-performance electrocatalyst for the hydrogen evolution reaction. *ACS Catal.* 8 (6), 5062–5069. doi:10.1021/acscatal.8b00949

Zhang, L., Mi, T., Ziaee, M. A., Liang, L., and Wang, R. (2018). Hollow POM@ MOF hybrid-derived porous Co_3O_4/$CoMoO_4$ nanocages for enhanced electrocatalytic water oxidation. *J. Mat. Chem. A* 6 (4), 1639–1647. doi:10.1039/C7TA08683K

Zhang, L., Peng, J., Zhang, W., Yuan, Y., and Peng, K. (2021). Rational introduction of borate and phosphate ions on $NiCo_2O_4$ surface for high-efficiency overall water splitting. *J. Power Sources* 490, 229541. doi:10.1016/j.jpowsour.2021.229541

Zhang, N., Feng, X., Rao, D., Deng, X., Cai, L., Qiu, B., et al. (2020). Lattice oxygen activation enabled by high-valence metal sites for enhanced water oxidation. *Nat. Commun.* 11 (1), 1–11. doi:10.1038/s41467-020-17934-7

Zhang, W., Lai, W., and Ca, R. (2017). Energy-related small molecule activation reactions: Oxygen reduction and hydrogen and oxygen evolution reactions catalyzed by porphyrin- and corrole-based systems. *Chem. Rev.* 117, 3717–3797. doi:10.1021/acs.chemrev.6b00299

Zhao, J., Ren, X., Ma, H., Sun, X., Zhang, Y., Yan, T., et al. (2017). Synthesis of self-supported amorphous CoMoO4 nanowire array for highly efficient hydrogen evolution reaction. *ACS Sustain. Chem. Eng.* 5 (11), 10093–10098. doi:10.1021/acssuschemeng.7b02093

Zheng, X., Zhang, B., De Luna, P., Liang, Y., Comin, R., Voznyy, O., et al. (2018). Theory-driven design of high-valence metal sites for water oxidation confirmed using *in situ* soft X-ray absorption. *Nat. Chem.* 10 (2), 149–154. doi:10.1038/nchem.2886

Zhi, W. S., Jakob, K., Colin, F. D., Ib, C., Jens, K. N., and Thomas, F. J. (2017). Combining theory and experiment in electrocatalysis: Insights into materials design. *Science* 355, eaad4998. doi:10.1126/science.aad4998

Zhu, Y., Yang, H., Lan, K., Iqbal, K., Liu, Y., Ma, P., et al. (2019). Optimization of iron-doped Ni_3S_2 nanosheets by disorder engineering for oxygen evolution reaction. *Nanoscale* 11 (5), 2355–2365. doi:10.1039/C8NR08469F

Zhuang, L., Ge, L., Yang, Y., Li, M., Jia, Y., Yao, X., et al. (2017). Ultrathin iron-cobalt oxide nanosheets with abundant oxygen vacancies for the oxygen evolution reaction. *Adv. Mat.* 29 (17), 1606793. doi:10.1002/adma.201606793